Experimental and numerical study of a micro-cogeneration Stirling unit under diverse conditions of the working fluid[☆]

G. Valenti[*]

gianluca.valenti@polimi.it

P. Silva

N. Fergnani

S. Campanari

A. Ravidà

G. Di Marcoberardino

E. Macchi

Politecnico di Milano – Dipartimento di Energia, Via R. Lambruschini 4A, 20156 Milano, Italy

*Corresponding author. Tel.: +39 02 2399 3845.

Abstract

Micro-cogeneration Stirling units are promising for residential applications because of high total efficiencies, favorable ratios of thermal to electrical powers and low CO as well as NO_x emissions. This work focuses on the experimental and the numerical analysis of a commercial unit generating 8 kW of hot water (up to 15 kW with an auxiliary burner) and 1 kW of electricity burning natural gas. In the experimental campaign, the initial pressure of the working fluid is changed in a range from 9 to 24 bar_g – 20 bar_g being the nominal value – while the inlet temperature of the water loop and its mass flow rate are kept at the nominal conditions of, respectively, 50 °C and 0.194 kg/s. The experimental results indicate clearly that the initial pressure of the working fluid – Nitrogen – affects strongly the net electrical power output and efficiency. The best performance for the output and efficiency of 943 W and 9.6% (based on the higher heating value of the burnt natural gas) are achieved at 22 bar_g. On the other hand, the thermal power trend indicates a maximum value of 8420 W at the working pressure of 24 bar_g, which corresponds to a thermal efficiency of 84.7% (again based on higher heating value). Measurements are coupled to a detailed model based on a modification of the work by Urieli and Berchowitz. Thanks to the tuning with the experimental results, the numerical model allows investigating the profiles of the main thermodynamic parameters and heat losses during the cycle, as well as estimating those physical properties that are not directly measurable. The major losses turn to be the wall parasitic heat conduction from heater to cooler and the non-unitary effectiveness of the regenerator.

Keywords: Stirling engine; Numerical modeling; Experimental testing; Micro-cogeneration; Micro-CHP

1 Introduction

In the scenario of micro-cogeneration (or micro Combined Heat and Power, micro-CHP), Stirling units are a promising technology for residential applications because of high total efficiencies, favorable ratios of thermal to electrical powers and lower emissions compared to reciprocating engines and micro gas turbines.[1] The present work covers the experimental and numerical analyses of a natural gas-fired commercial unit capable of generating 8 kW of hot water (up to 15 kW with an auxiliary burner) and 1 kW of electricity. Although featuring in general a low electrical efficiency, these micro-cogeneration units are able to recover heat with a high thermal efficiency, thus qualifying positively in terms of primary energy savings. Moreover, the thermal-to-electrical power ratios of 8-to-1 (and 15-to-1 with the additional burner) are well suited for covering simultaneously the thermal and electrical loads of typical residences in continental climates.

Chen and Griffin [1] as well as Cheng and Yu [2] conduct two detailed reviews of the numerical investigations on Stirling engines in 1983 and in 2010, respectively. Among these investigations, the work by Urieli and Berchowitz provides a fundamental contribution in 1977 [3]. Their numerical model, especially the so-called "simple analysis" variant, represents a balanced compromise between simplicity, accuracy and generality for the calculation of the performance of any

Stirling engine.

The first study investigating the heat transfer phenomena inside the engine, which influence strongly the engine performance, is likely that by Finkelstein and Organ [4]. The authors develop a specific approach to quantify the regenerator heat exchange and to include the effects of a compressible working fluid in the estimation. Shultz and Schwendig [5] propose a simulation model of the general Stirling cycle. A further development is the work by Kongtragool and Wongwises [6], which studies the effects of dead volumes by manufacturing and testing twin- and four-piston engines.

In later years, Karabulut investigates specifically the beta free piston engines [7], whereas Parlak et al. deal with the gamma engine under almost stationary flow conditions [8], and Andersen et al. develop a one-dimensional model [9]. The first computational fluid-dynamics models are realized probably by Organ [10] and by Mahkamov [11], whose numerical results indicate clearly that the fluid-dynamic losses within the regenerator and the "dead" volumes are the major factors reducing the power output from the engine. Timoumi et al. [12] prove that the actual engine efficiency remains very low compared to the high theoretical value. Several engine losses are identified by Walker [13] and by Wilson et al. [14]: conduction losses in the heat exchangers, dissipation by pressure drop, shuttle and gas spring hysteresis losses. Costea et al. [15] highlight how the irreversibility due to heat transfer and pressure drop in the thermodynamic cycle has a significant importance in predicting the performance of the engine itself.

Regarding the regenerator of the Stirling engine, which affects majorly its performance, Gedeon and Wood provide a fundamental work in 1996 [16]. The authors verify experimentally the heat exchange and the pressure drop inside wowed matrix regenerators under oscillating flow conditions and, consequently, formulate a full set of empirical correlations. Later, Costa et al. confirm these correlations by numerical means [17]. Recently, Cheng and Yang [18] analyze the effects of the geometrical parameters on the shaft work for alpha, beta and gamma engine configurations. The simulation of the reference alpha engine yields a maximum shaft work for a phase angle shift of 80° and a dead to swept volume ratio of 0.5 (these parameters are close to the ones of the engine studied in this work).

If the open literature has plenty of numerical predictions of Stirling engine performance, it appears not to be as rich of experimental verifications of the actual performances. Aliabadi et al. examine the efficiency and the emissions of a residential Stirling engine fueled by diesel and biodiesel. Regarding specifically the electrical efficiency, the authors report it is around 11.5% with respect to heating values determine by ASTM D4809 standard [19]. That engine is the preceding version of the one used in this work and is fed by a liquid fuel instead of natural gas. Lastly, García et al. test the performances of two alpha engines under several working pressures and carry out a comparison among different numerical models [20]. They report a mechanical and an alternator efficiencies falling respectively in the range of 62–80% and 68–90% and depending mainly on the mechanical power output, which in its turn depends upon the mean pressure of the working gas.

As part of an ongoing study [21], a second campaign on the above-mentioned natural gas-fueled commercial Stirling unit is carried out at the Laboratory of Micro-Cogeneration of Politecnico di Milano [22]. The objective is to collect experimental data under diverse initial pressures of the working fluid, taking measurements at the boundary of the engine as well as inside the engine itself. The data are employed to reconstruct mass and energy balances and to assess energy and emission performances. They are also used to tune an in-house numerical model that is utilized ultimately to evaluate several parameters that are not accessible by direct measurement. To the knowledge of the authors, studies that are both numerical and experimental about Stirling engines are not common in the literature and, furthermore, there are no studies about diverse pressures of the working fluid.

The following sections illustrate first the experimental setup and then the numerical model. Next, the results from the experimental campaign as well as of the tuned numerical code are reported. Finally, conclusions are drawn.

2 Experimental campaign

The experimental campaign aims at creating a databank of measurements and at evaluating the performances in terms of electric and thermal efficiencies as well as of emissions upon the change of the initial pressure of the working fluid, Nitrogen (where "initial" indicates prior to starting up the unit). The initial pressure of Nitrogen is varied in discrete steps, 9, 12, 16, 20 (the nominal value), 22 and 24 bar_g. Other main parameters are instead kept constant, as described below. A high purity Nitrogen, of 5.0 quality, is employed in the campaign.

The experimental setup, shown in Fig. 1, provides measurements taken both externally and internally to the Stirling unit. Regarding the fed gases, which are natural gas from the national grid and the ambient air, the setup allows acquiring the inlet temperature and pressure. For the sole natural gas, also mass flow rate as well as molar composition with a micro gas chromatograph are collected. The temperature of air required for the combustion is controlled by a heating, ventilating, and air conditioning system (with a specified set point of 25 °C in this campaign). Regarding the flue gas, the measures include temperature, specific emissions (CO, NO, NO_2, SO_2) with an electrochemical analyzer, and molar composition with the same gas chromatograph adopted for the natural gas. A great attention is paid to the value of O_2 measured by both the analyzer and the gas chromatograph. For the water loop, temperatures, pressures, differential pressure and mass flow rate are acquired. In particular, the inlet flow rate of the water loop is managed by way of a variable-speed pump (set point of 0.194 kg/s); similarly, the inlet temperature is managed by a controlled-valve system (set point of 50 °C). The other external instruments are an electric power analyzer and a load cell to weight the condensate water from the flue gas. Nitrogen initial pressure, water inlet temperature and water mass flow rate define a single operating condition of the campaign.
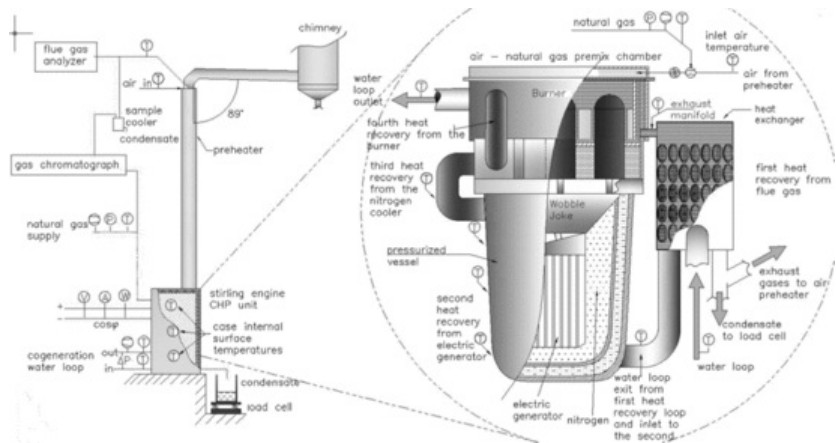
Fig. 1 Scheme of the experimental setup showing the measurements acquired internally and externally to the engine.

Internally, on the air side, temperature is measured at the inlet of the engine after the air preheater and, on the flue gas side, at the outlet of the engine before entering the preheater itself. A thermocouple is placed in contact with one piston crown to detect the highest temperature of the cycle, namely the heater wall temperature (which is an important parameter for the numerical model). Thermoresistances on the water loop allow determining heat exchanges in the four main stages (refer to Fig. 1). Thermocouples are also placed on the engine walls. All instruments, external and internal, are outlined in Table 1.

Table 1 Instrumentation complete of manufacturer, model and uncertainty (FS stands for full scale, RV for read value) employed in the experimental campaign.

Property and location	Manufacturer	Model	Uncertainty
Temperature			
Water (inlet/outlet)	Scandura	Pt100 4 wires	1/3 DIN
Water (internally)	Tc direct	Pt100 4 wires	1/10 DIN
	Tc direct	Self-adhesive type T	Class 1
Exhaust (outlet)	Scandura	Pt100 4 wires	1/3 DIN
Exhaust (internally)	Tc direct	type K	Class 1
	Tersid	type K	Class 1
	Tc direct	Pt100 4 wires	1/10 DIN
Natural gas	Tc direct	Pt100 4 wires	1/10 DIN
Wall	Tc direct	Self-adhesive type T	Class 1
	Tc direct	Eyelet type T	Class 1
	Tc direct	type K	Class 1
Mass flow rate			
Water loop	Emerson	Micromotion Coriolis Elite CMF025	±(0,1% RV)
Natural gas	Bronkhorst	IN-FLOW 112-AI	±(0,5% RV + 0,1% FS)

| Weight			
Condensate water	Laumas	Load Cell-TLS420	±0.25 g
Ambient			
Pressure	Vaisala	PTU300	±0.15 hPa
Temperature	Vaisala	PTU300	±0.10 °C
Relative humidity	Vaisala	PTU300	±1.0% RH @40…97% RH
Pressure			
Nitrogen	Spriano	Manometer	±(0.25% FS)
Natural gas	Bronkhorst	IN-PRESS P-502CI	±(0.5% FS)
Water loop	Rosemount	2088 A	±(0.1% FS) @ 0.1…10 bar
Differential pressure			
Water loop	Rosemount	2051 CD	±(0.075% FS) @ 0…2.6 bar
Emissions	Testo	Testo 360	O_2: ±(0.2%pt RV)
			CO/H_2: ±50 ppm
			NO, NO_2, SO_2: ±10 ppm
Gas composition	Pollution	VEGA-GasCromatograph 30003 columns Cpsil, Molsieve, PPQ	2% on each species (but methane 0.2%)
Electric power	Fluke	NORMA 4000	±0.1% RV

After the system reaches a steady state condition, measures are acquired every 2 s, but emissions from the electrochemical analyzer that are acquired every 30 s and compositions from the micro gas chromatographer every about 3 min. The steady state condition is verified observing the variation of the engine electrical power generation, which must remain within a ±10 W band, and the water loop inlet and outlet temperatures, which must remain within ± 0.4 °C band. During steady state, the overall system shows actually a negligible oscillation with a period of 30–60 min. The time span of the data acquisition is taken to be equal to 2 oscillations of the overall system and, thus, it is typically from 1 to 2 h. This time span is also long enough to collect an appreciable amount of condensate that is weighted. Then, the recorded data are filtered statistically prior to determine their mean values. The mean values are ultimately used to evaluate mass and energy balances as well as cogeneration unit and engine net electrical and thermal efficiencies. Tests on a single operating condition are repeated at least nine times over at least two days in order to verify the repeatability of the measurements.

3 Numerical model

The numerical model developed in this study is a modification of the well-known work by Urieli and Berchowitz [3]. The Stirling engine is divided into five different cells, as visualized in Fig. 2. From left to right, the cells are: (c) fluid compression, (k) cooling, (r) regeneration, (h) heating, and (e) expansion. The simulation procedure includes in sequence:

- splitting one full engine revolution into short steps (e.g. 10° of shaft revolution);

- computing the mass content and the thermodynamic conditions (i.e. temperature, pressure, specific volume and enthalpy) inside each cell and for each step. Within each step, the conditions of any cell are assumed to be stationary while the variation from one step to the following one is evaluated according to the equations of the Urieli model, which is briefly recalled in Appendix A.

- calculating the gas transfer flow between neighboring cells and heat/work exchanged through the walls/pistons of the engine for each step, according to the energy equations presented in Appendix A.

- integrating the cited head/work exchanged over one shaft revolution to evaluate the performances (e.g. heat power input, mechanical power transferred to the shaft, heat rejected to the cooler).
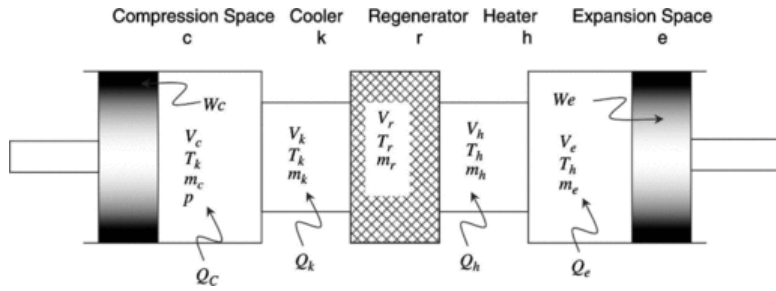
Fig. 2 Scheme showing the five cell used in the numerical model of the engine.

The whole process is iterated by varying the initial thermodynamic conditions of the cells, until the difference between the first and the last computational step (referred to the same position of the engine shaft) is lower than a given threshold.

The thermodynamic processes inside the compression and expansion cells are assumed to be adiabatic, which is an assumption much closer to reality than the isothermal approximation related to the ideal Stirling cycle. In fact, since expansion and compression are very fast and take place in a section of the engine that is not designed to promote heat exchange, the heat exchanged through the walls of the pistons is negligible. In addition, the temperatures inside the cooling and heating cells are taken to be uniform within each step. With respect to the original model [3], this work includes several novel subroutines to predict the following parameters:

- thermal behavior of the metal screen regenerator under oscillating flow conditions;

- irreversibility of the exchanged heat within the heater and cooler cells due to temperature differences;

- concentrated and distributed pressure losses within heater, cooler and regenerator cells;

- heat losses due to conduction from the heater to the cooler cell through the walls;

The physical approach adopted in each routine is outlined in the Appendix A. Pressure losses tend to be large due to the extension and tortuosity of the exchange surface. The losses generated by the friction of the fluid flow, called "pumping losses", have a direct effect in terms of reducing the cycle useful work. Conceptually, the frictional losses occurring in the cooler and in one semi-volume of the regenerator cause an increase in compression work, while those occurring in the heater and in the other semi-volume of the regenerator cause a reduction of expansion work. On top of this, the work dissipated due to pumping losses causes an additional heating of the working fluid, which reduces the heat introduced through the heater but increases the one removed through the cooler.

For a given set of temperatures of the heater wall and the cooling water inside the cooler ducts, the non-ideality of both the exchanged heat inside the heater and the cooler yields a decrease of the gas temperature inside the heater, along with an increase of the gas temperature inside the cooler. For each simulation step, the temperature differences between gas and walls/water are evaluated by means of heat exchange coefficients, assuming forced convection conditions at variable gas speed inside the ducts.

Lastly, the incidence of mechanical losses within the wobble yoke and the bearings as well as the electrical losses due to the non-ideal generator and auxiliary power drain are evaluated from the work of Garcìa et al. [20] and of the authors [21].

The prediction of heat exchange phenomena and of temperature evolutions inside the engine are based on gas speeds and pressures, which are firstly guessed through a numerical simulation where the heat exchanges are assumed to be ideal. An iterative algorithm, depicted in Fig. 3, is adopted to converge to the non-ideal values. The model describes the behavior of a single compressor-cooler-regenerator-heater-expander volume, as highlighted in Fig. 4, while the engine comprises four cylinders arranged on a circular disposition. Hence, the Stirling engine is simulated by combining the four contributions shifting the results of a single cylinder along a sinusoidal path. Finally, the model is able to solve the mass and energy balance occurring in every cylinder during one shaft revolution. Furthermore, it allows investigating several thermodynamic parameters evolving within the engine during the cycle, along with the most relevant energy dissipations that affect the engine electrical efficiency.
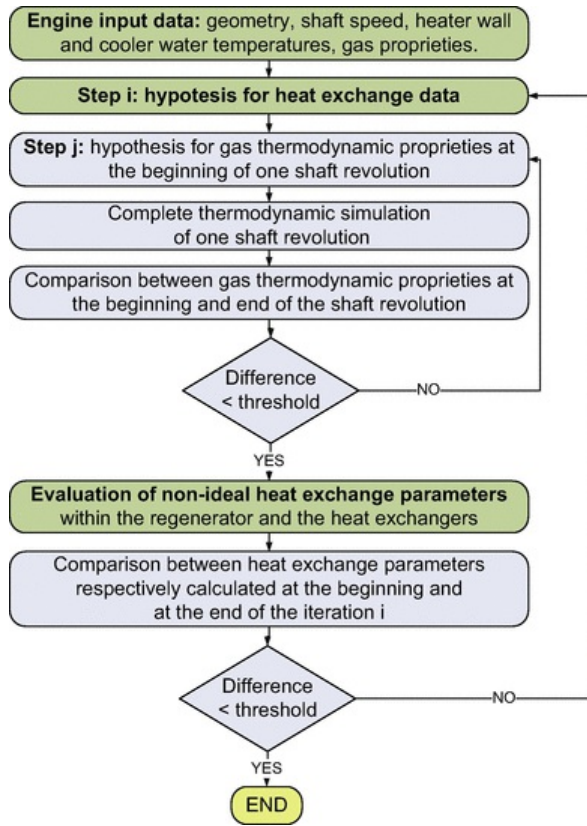
Fig. 3 Flow diagram of the algorithm developed to solve the numerical model.
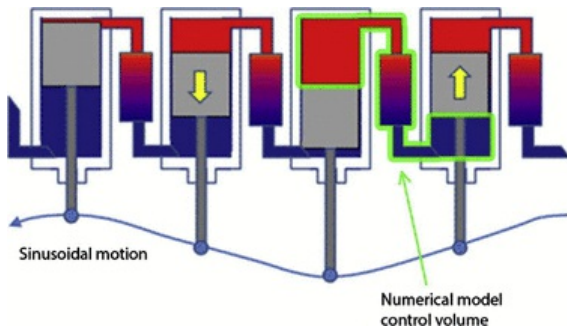

Fig. 4 Cylinders connection scheme and highlight of the control volume studied within the numerical model.

The input information for the simulation includes the complete geometry of the engine and of the heat exchangers, in addition to the composition and the nominal initial pressure of the gas, the operating temperatures and the shaft speed. Table 2 shows the set of input data used in this work. The geometry is defined according to direct measurements of few parts of the engine and to assumed values of the inaccessible parts. All data are taken constant for every simulation, exception made for the cooler water temperature, the heater wall temperature and the gas pressure that are varied according to the operating conditions and the experimental campaign.

Table 2 Numerical values of the input data for the simulation. Data are related to a single working volume (compressor–cooler–regenerator–heater–expander), i.e. a single cylinder among the four cylinders of the engine.

Engine		Regenerator	
Type	Wobble yoke	Type	Annular
Compression space clearance volume (cm^3)	19.1	External annulus outer diameter (m)	0.0636
Compression space swept volume (cm^3)	27.4	External matrix diameter (m)	0.0566
Expansion space clearance volume (cm^3)	19.9	Internal matrix diameter (m)	0.0435
Expansion space swept volume (cm^3)	28.4	Internal annulus inner diameter (m)	0.0415
Wobble yoke arm length (m)	0.0725	Length (m)	0.02
Cylinder stroke (m)	0.021	Matrix type	Porous media
Expansion space phase angle advance (°deg)	90	Porosity	0.698
Engine speed (Hz)	25	Wire matrix diameter (m)	6.00E−05
Mechanical losses @ 25 Hz (W)[a]	53	Total matrix wet surface (m^2)	0.35
Generator electrical efficiency[a]	0.90	Matrix screen width (m)	2.16E−04
Auxiliary average power drain (W)[a]	15	Number of cross section wires	6367
Cooler		Heater	
Type	Fins	Type	Fins
Length (m)	0.052	Length (m)	0.049
Number of fins	180	Number of fins	84
Fins height (m)	0.0018	Fins height (m)	0.003
Fin-to-fin width (m)	5.55E−04	Fin-to-fin width (m)	5.00E−04
Cooler average cross section (m^2)	1.80E−04	Heater average cross section (m^2)	1.26E−04
Sum of cooler concentrated loss factors	4	Sum of heater concentrated loss factors	4
Data from the experimental campaign			
Working gas type	Nitrogen (5.0)	Cooler average water temperature (°C)	See Table 4
Working gas initial pressure (bar_g)	See Table 4	Heater wall temperature (°C)	See Table 4

[a] Evaluated in previous works [21].

4 Results

Table 3 shows the main results from the experimental campaign. All reported values are the mean of at least nine tests conducted on a single operating condition. The natural gas input, defined with respect to the fuel higher heating value (HHV), has a maximum at 24 bar_g with 9940 W compared to 9850 W at 20 bar_g and 8720 W at 9 bar_g. The same trend is observed for thermal power output, whose values vary from 7850 W at the lowest pressure to 8420 W at the highest. Similarly, the higher the pressure the higher the net electrical power output, from 418 W at 9 bar_g to 943 W at 22 bar_g, even if, as explained below, a minor decrease to 942 W is recorded at the highest pressure step (such small decrease is anyhow greater than the instrument uncertainty). Regarding the efficiencies, the net electrical efficiency of the unit increases from 4.8%, always based on the higher heating value of the fuel, to 9.6%. However, the thermal efficiency has a minimum at high pressures with 84.7% compared to 90.0% at 9 bar_g and 85.9% at 16 bar_g. The total efficiency is almost constant and falls in the range from 94.1% to 94.8% for all cases.

Table 3 Main experimental measures of the Stirling unit for the different Nitrogen initial pressure. (HHV stands for the fuel higher heating value.).

Parameters	Experimental					
Working gas initial pressure (bar$_g$)	9	12	16	20	22	24
Fuel input to unit (HHV) (W)	8720	9260	9680	9850	9860	9940
Engine/unit electrical power output (W)	418	613	809	909	943	942
Thermal output from unit (W)	7850	8130	8320	8350	8360	8420
Net electric efficiency of unit (HHV, %)	4.8%	6.6%	8.4%	9.2%	9.6%	9.5%
Thermal efficiency of unit (HHV, %)	90.0%	87.8%	85.9%	84.9%	84.7%	84.7%
Total efficiency of unit (HHV, %)	94.8%	94.5%	94.2%	94.1%	94.3%	94.2%

For all the tested operating conditions, an error analysis is conducted following the ISO/IEC Guide 98 – Part 3 [23]. This analysis demonstrates that the instrument relative uncertainty on the net electrical power output is ±0.1% and that the combined relative uncertainty for the natural gas input (defined with respect to the higher heating value) is around ±0.9% and for the thermal power output is around ±2.7%. Consequently, the combined relative uncertainties for the net electrical efficiency and the thermal efficiency are about ±1.0% and ±3%, respectively, which correspond to combined (absolute) uncertainties of approximately ±0.1%-points on the electrical efficiency and ±2.8%-points on the thermal efficiency.

Table 4 reports a comparison between experimental and numerical results for three selected Nitrogen initial pressures out of the five considered in the campaign: 12 (low-pressure), 20 (nominal) and 24 bar$_g$ (high-pressure case). The numerical model provides an analysis of the Stirling engine only, while experimental data refers to the Stirling unit including the natural gas burner, fan, the engine itself, the heat recovery from the cooled-side of the engine and the heat recovery from the exhausts. Measured and predicted net electrical powers for the selected cases are in a good agreement. As explained and discussed below, measurements and predictions differ by an almost constant bias.

Table 4 Comparison among result of the experimental campaign and numerical model output for three selected operating conditions out of the five considered in this work: low-, nominal- and high-pressure cases. Experimental values are the mean of the at least nine tests conducted on each operating condition. (Sim stands for simulated, Exp for experimental, Diff for difference, and HHV for the fuel higher heating value.).

Parameters	Sim.	Exp.	Diff.	Sim.	Exp.	Diff.	Sim.	Exp.	Diff.
Working gas initial pressure (bar$_g$)	12			20			24		
Heater wall temperature (°C)	610			532			499		
Cooler wall temperature (°C)	98			105			116		
Heat input to engine (W)	4961	–		6146	–		6643	–	
Heat rejected from the cooler (W)	3917	–		4763	–		5220	–	
Gross mechanical power (W)	1044	–		1382	–		1422	–	
Heat loss due to piston stroke (W)	203	–		170	–		152	–	
Heat loss due to wall conduction (W)	2034	–		1696	–		1520	–	
Pumping loss (W)	69	–		104	–		121	–	
Heat loss due to non-ideal regenerator (W)	465	–		758	–		860	–	
Mechanical frictional loss (W)	212	–		212	–		212	–	
Generator energy loss (W)	83	–		117	–		121	–	
Auxiliary power absorption (W)	60	–		60	–		60	–	

Engine/unit electrical power output (W)	689	613	−12.4%	993	909	−7.1%	1029	942	−9.2%
Engine electrical efficiency (%)	13.9%	—		16.2%	—		15.5%	—	
Fuel input to unit (HHV) (W)	—	9260		—	9850		—	9940	
Thermal output from unit (W)	—	8130		—	8350		—	8420	
Thermal efficiency of unit (HHV, %)	—	87.8%		—	84.9%		—	84.7%	
Net electric efficiency of unit (HHV, %)	—	6.6%		—	9.2%		—	9.5%	
Total efficiency of unit (HHV, %)	—	94.5%		—	94.1%		—	94.2%	

The numerical results of Table 4 show that heat losses related to piston stroke and wall conduction decrease when the pressure rises, despite the higher heat transfer coefficient between the compressed gas and the engine walls, because of a decrease of the temperature difference between heater and cooler walls. On the other side, there is an increase of pumping and regenerator losses, due to the higher density of the working gas. Moreover, the electrical efficiency of the engine increases when the pressure rises from 12 to 20 bar_g, owing to a relative decrease of fixed losses, and decreases slightly from 20 to 24 bar_g, mainly owing to the lower heater temperature and higher cooler temperature.

Fig. 5 depicts the measured and simulated trends of the net electrical power output over the whole range of Nitrogen initial pressures considered in this work. The labels indicate the measured heater wall temperatures, which have an important influence over the simulation outcomes. The numerical predictions follow closely the ascending trend of the experimental measures. However, an underperformance of the experimental electrical output ranging from 50 to 80 W can be observed for all pressures. For instance, the electrical output at the nominal 20 bar_g is just 909 W compared to a nominal rate of (almost) 1000 W. This underperformance is probably due to wear and aging of the Stirling unit, which has been subjected to many tests and modifications to allow for the internal measurements.
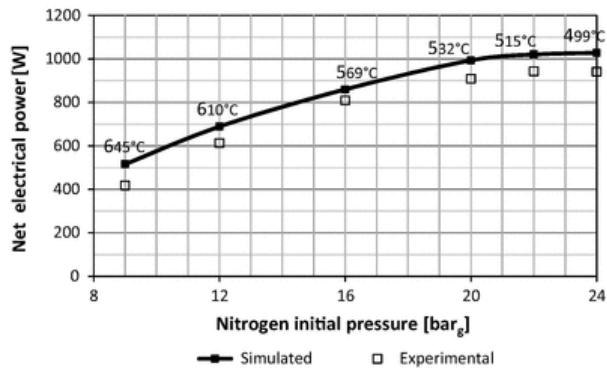

Fig. 5 Experimental and simulated engine net electrical power and efficiency as a function of Nitrogen initial pressure from 9 to 24 bar_g (labels indicate the measured heater temperatures).

Table 5 reports a simulation of the non-ideal behavior of the heat exchangers for the nominal case of 20 bar_g. The gas-wall temperature difference inside the heater is almost twice as much that inside the cooler. This difference is primarily due to the greater heat flow in the first component as compared to the second one. Secondly, the greater density of the fluid passing through the cooler, along with the presence of smaller sized ducts, results in a greater convective coefficient. The high average gas temperature inside the cooler, as compared to the cooling water temperature (50 °C), is also related to the non-ideal heat exchange through the cylindrical walls of the cooler and from the external finned wall to the cooling water. In addition, generally speaking, the axial conduction losses through the regenerator walls cause a high thermal loss, mainly due to the great temperature difference between cooler and heater, as well as to the high thermal conductivity of the metal and to the high average thickness necessary to overcome the pressure stress. Likewise, Table 6 shows the results from the analysis of the losses due to the pressure drops for the nominal case of 20 bar_g. These losses take place in the connection conduits between the different sections of the engine, in the heat exchangers and in the regenerator. Pumping losses resulting from the simulation are as low as 7.5% of the 1382 W mechanical gross power output, mainly due to the low gas speed in all the sections of the engine.

Table 5 Numerical heat exchange results for the 20 bar_g operating condition (four-cylinder engine).

Regenerator

Regenerator heat losses	868.8 W
Wall conduction heat losses	1978 W
Cooler	
Average gas temperature inside cooler	127.1 °C
Average gas-wall temperature difference	22.5 °C
Heater	
Average gas temperature inside heater	491.7 °C
Average gas-wall temperature difference	40.3 °C

Table 6 Numerical pressure drop results for the 20 bar$_g$ operating condition (four-cylinder engine).

Pressure drop	
Average cooler	2425 Pa
Average regenerator	8209 Pa
Average heater	6196 Pa
Pumping loss	
Average cooler	16.4 W
Average regenerator	41.6 W
Average heater	41.6 W
Total	99.6 W

The numerical model also allows studying several thermodynamic parameters evolving within the engine during the cycle, such as: gas temperatures and speeds, Reynolds numbers, heat exchange coefficients, pressure drops, pressure inside compression and expansion space. Fig. 6 shows the pressure inside compression and expansion spaces over one shaft revolution, along with the pressure values related to a cycle not affected by the pumping losses. The compression work increases due to the pressure drops, while expansion work is reduced. The difference between the area respectively included in the expansion pressure curve (which goes clockwise) and the compression curve (which goes counterclockwise) gives the gross mechanical power of the cycle.
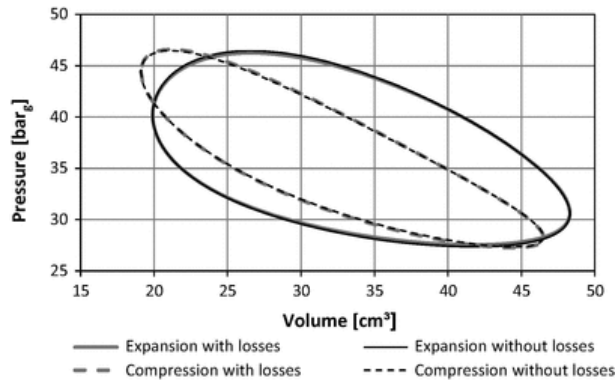
Fig. 6 Pressure inside compression and expansion space calculated without pressure drops (thin and blank lines) and with pressure drops (thick and gray lines).

Another way to summarize the energy flows occurring in one shaft revolution is presented in Fig. 7, where the cumulated energy transferred within the heater, cooler, regenerator, expansion piston and compression piston is depicted. For a complete shaft revolution the integral of the heat introduced through the heater is positive, while the one related to the cooler is negative. The integral of the heat exchanged by the regenerator is equal to zero, provided that under regime conditions all the heat absorbed by this component during the heater-to-cooler mass transfer is rejected during the cooler-to-heater mass transfer. The solid line represents the useful work, computed as the difference between the integral of expansion and compression work.
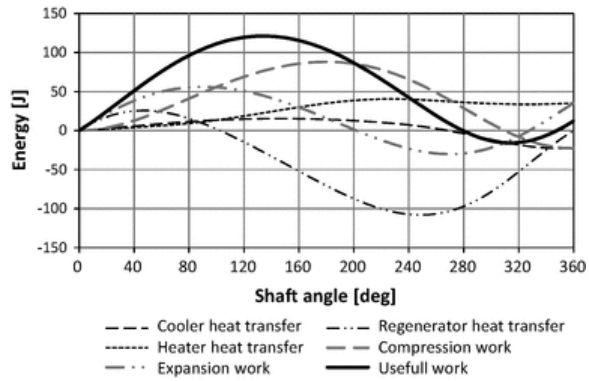

Fig. 7 Cumulated energy exchanged over one shaft revolution.

Finally, Fig. 8 shows the measured emissions of CO and NO_x, defined at 6% oxygen content in the dry exhausts, over the considered Nitrogen initial pressures. CO emission slightly increases with pressure from 15 to 25 ppm, likely due to the lower wall temperatures within the combustion chamber, whereas NO_x remains roughly constant around the value of 15 ppm. Data for the sole case at 24 bar$_g$ are missing due to an instrument failure. For comparison, emissions from micro gas turbines are at similar levels with CO and NO_x falling typically in the range 10–20 ppm for dry exhausts at 15% oxygen, which is equivalent to 25–50 ppm at 6% oxygen. In contrast, emission from internal combustion engines can be as high as a few hundreds if proper abatement system are not installed, as reported by Thomas [24].
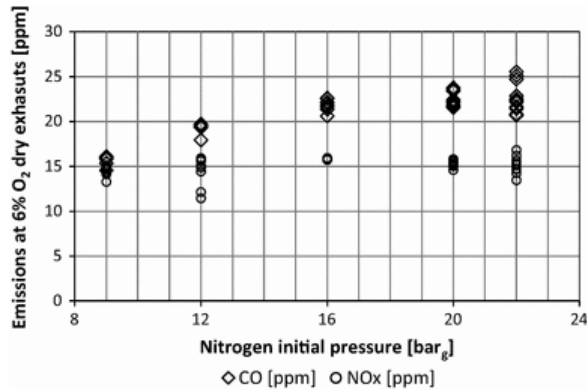
Fig. 8 Experimental emissions (CO, NO$_x$), defined at 6% oxygen content in the dry exhausts, as a function of Nitrogen initial pressure. Data for 24 bar$_g$ are missing due to an instrument failure.

5 Conclusions

The present work covers both an experimental campaign and a numerical study on a micro-cogeneration Stirling unit for residential application. The unit is analyzed varying of the initial pressure of the working fluid, Nitrogen. The experimental data are used to reconstruct mass and energy balances as well as to compute electrical and thermal efficiencies of the cogeneration unit. Moreover, they are adopted to tune the numerical model, which can be employed ultimately to estimate physical properties that are not directly measurable. The work derives the following conclusions.

- The working fluid pressure has a positive impact on the electric power production that reaches a maximum measured value of 943 W at 22 bar$_g$, which corresponds to a net electric efficiency of the cogeneration unit equal to 9.6%, based on the fuel higher heating value. At 24 bar$_g$ the recorded power generation is slightly lower and equal to 942 W, corresponding to a net electric efficiency of 9.5%

- The numerical model shows an almost-constant predicted electrical power of 1020~~to~~ 1028 W in the range from 22 to 24 bar$_g$ and a maximum value of the net electrical efficiency of 16.6% (Stirling engine only) at 20 bar$_g$.

- Numerical results for the net electric power output over the whole range of the Nitrogen initial pressures follow closely the trend of experimental data. Nevertheless, a bias ranging from 50 to 80 W can be observed for all pressures. The experimental underperformance could be due to wear and aging of the tested unit.

- The measured thermal power transferred to the heat recovery water loop has a maximum at 24 bar$_g$ with 8420 W. On the other hand, the thermal efficiency has an opposite trend with the minimum value of 84.7% at high pressures.

- The total efficiency remains relatively constant for all the tested conditions and falls in the range from 94.1% to 94.8%.

- For all cases, since the instrument relative uncertainty of the electric power analyzer is just 0.1%, the error propagation analysis shows that the combined relative uncertainty for the net electrical efficiency is about ±1.0%, corresponding to an (absolute) uncertainty of about ±0.1%-points. Since the relative uncertainty of the water loop temperature difference is as high as 2.7%, the combined relative uncertainty for the thermal power output is around ±2.7%. Consequently, the combined relative uncertainty for the thermal efficiency is ±3%, corresponding to an (absolute) uncertainty of about ±2.8%-points. This is mainly due to the thermoresistances (Class 1/3 DIN) on the outside of the Stirling unit. In the next campaigns, they will be replaced with high precision probes (Class 1/10 DIN).

- The numerical model allows investigating the losses within Stirling engine and the evolution of the main thermodynamic parameters during the cycle, which are not measureable. In particular, the non-ideal behavior of the heat exchangers, the regenerator, the losses due to the thermal conduction and pressure drops are analyzed in the whole range of pressures. The major losses are related to the wall conduction and to the non-ideal behavior of the regenerator.

Acknowledgements

Appendix A. Model summary

This appendix replicates the equations employed in the well-known model by Urieli and Berchowitz and it outlines those implemented in this work to improve that model. The appendix is meant for a reader familiar with the modeling of Stirling engines.

A.1 Ideal adiabatic model by Urieli and Berchowitz

The box in Fig. 9 outlines the equations developed by Urieli and Berchowitz [3]. These equations allow to evaluate the thermodynamic parameters of the gas within each cell and for each step of the complete shaft revolution. They are sorted into groups of thermodynamic properties. The last group of equations refers to the heat and the work respectively transferred from gas to engine walls and from gas to pistons. The used acronyms are: (c) fluid compression, (k) cooling, (r) regeneration, (h) heating, and (e) expansion.

$p = M R / (Vc / Tc + Vk / Tk + Vr / Tr + Vh / Th + Ve / Te)$ $dp = \dfrac{-\gamma\, p\, (dVc / Tck + dVe / The)}{[Vc / Tck + \gamma(Vk / Tk + Vr / Tr + Vh / Th) + Ve / The\,]}$	Pressure
$mc = p\, Vc / (R\, Tc)$ $mk = p\, Vk / (R\, Tk)$ $mr = p\, Vr / (R\, Tr)$ $mh = p\, Vh / (R\, Th)$ $me = p\, Ve / (R\, Te)$	Masses
$dmc = (p\, dVc + Vc\, dp / \gamma) / (R\, Tck)$ $dme = (p\, dVe + Ve\, dp / \gamma) / (R\, The)$ $dmk = mk\, dp / p$ $dmr = mr\, dp / p$ $dmh = mh\, dp / p$	Mass Accumulations
$mck' = -dmc$ $mkr' = mck' - dmk$ $mhe' = dme$ $mrh' = mhe' + dmh$	Mass Flow
if $mck' > 0$ then $Tck = Tc$ **else** $Tck = Tk$ if $mhe' > 0$ then $The = Th$ **else** $The = Te$	Conditional Temperatures
$dTc = Tc\, (dp / p + dVc / Vc - dmc / mc)$ $dTe = Te\, (dp / p + dVe / Ve - dme / me)$	Temperatures
$dQk = Vk\, dp\, cv / R - cp\, (Tck\, mck' - Tk\, mkr')$ $dQr = Vr\, dp\, cv / R - cp\, (Tk\, mkr' - Th\, mrh')$ $dQh = Vh\, dp\, cv / R - cp\, (Th\, mrh' - The\, mhe')$ $dWc = p\, dVc$ $dWe = p\, dVe$ $dW = dWc + dWe$ $W = Wc + We$	Energy

Fig. 9 Box outlining the equations by Urieli and Berchowitz [3].

A.2 Non-ideal thermal behavior of the regenerator

The heat losses caused by the non-unitary effectiveness of the regenerator ($\dot{Q}_{loss,reg}$) are evaluated according to the empirical expression given by Gedeon and Wood [16], who verified experimentally the heat exchange and the pressure drop inside wowed matrix regenerators under oscillating flow conditions. Because of its experimental origin, the expression includes losses resulting from: non-ideal heat exchange between gas and metal screens, axial conduction of metal screen and axial conduction of gas (which is anyhow almost negligible). Such loss can be computed as:

$$\dot{Q}_{loss,reg} = \frac{0.194 \cdot (Re_{max} \cdot \overline{Pr})^{1.3}}{\phi^{1.81}} \cdot \lambda_f \cdot S \cdot \Delta T_r \cdot \frac{1}{L_r}$$

where Re_{max} is the maximum Reynolds number ascribed to the gas during one shaft revolution (evaluated in the adiabatic analysis), $\overline{Pr}$ is the Prandtl number of the working fluid evaluated at a mean temperature, ϕ the porosity of the regenerator (void volume over total volume of regenerator), λ_f the thermal conductivity of the gas, S the average gas flow free section, ΔT_r the average difference between the temperature of gas inside heater and cooler, and L_r the axial length of the regenerator.

A.3 Non-ideal thermal behavior of heater and cooler

The temperature of the gas leaving the heater and the cooler (constant during the cycle) is respectively lower and higher than the associated wall temperature due to the non-ideality of the heat exchange. Assuming a positive sign for the heat flow transferred to the gas ($\dot{Q}_{in}$), the gas temperature (T_{gas}) is evaluated as:

$$T_{gas} = T_{wall} - \frac{\dot{Q}_{in}}{h_{avg}A_i}$$

where h_{avg} is the average heat exchanger coefficient evaluated according to Reynolds relation within one shaft revolution. For each step of the shaft, the instantaneous heat transfer coefficient (h_i) is:

$$h_i = \frac{fr \cdot \mu \cdot \overline{c_p}}{2 \cdot D_y \cdot Pr^{2/3}}$$

where D_y stands for the hydraulic diameter of the heater or of the cooler ducts, Pr and μ respectively for Prandtl number and dynamic viscosity evaluated as a function of the gas temperature, $\overline{c_p}$ for the gas specific heat coefficient evaluated at a mean temperature and fr for the Fanning friction factor. This last term is evaluated assuming a fully developed turbulent flow, resulting from the hi-speed of the gas inside the ducts, that is:

$$fr = 0.0791 \cdot Re^{0.75}$$

A.4 Friction losses within heater, cooler and regenerator

The main effect of friction losses is the reduction of the useful work extracted from the engine. While heater and cooler friction losses could be associated respectively to a reduction in the expansion work and an increase of the compression work, the losses related to the regenerator are split into two equal parts, respectively allocated to expansion and compression work. Mathematically, useful work extracted from the engine at each revolution (W) is:

$$W = \oint p\,dV_c - \oint \left(\Delta p_k + \frac{1}{2}\Delta p_r\right)dV_c + \oint p\,dV_e - \oint \left(\Delta p_h + \frac{1}{2}\Delta p_r\right)dV_e$$
$$= W_{ideal} - \oint \left(\Delta p_k + \frac{1}{2}\Delta p_r\right)dV_c - \oint \left(\Delta p_h + \frac{1}{2}\Delta p_r\right)dV_e$$

where the dV indicates the variation of volume for the expansion (*e*) and the compression (*c*). The terms Δp are instead the instantaneous pressure drops for cooler (k), regenerator (r) and heater (h), evaluated for each shaft step as follows:

$$\Delta p = f_d \cdot \frac{L}{D_y} \cdot \frac{\rho u^2}{2}$$

where D_y stays for hydraulic diameter heat exchangers (heater, cooler or regenerator), ρ and u respectively for density and instantaneous speed of the gas and f_d for the Darcy friction factor. This last term is evaluated according to the classic circular pipe correlations for the heater and the cooler, whereas for the regenerator the experimental formulation given by Gedeon and Wood [16] is used:

$$f_{d,reg} = \frac{129}{Re} + 2.91 \cdot Re^{-0.103}$$

A.5 Parasitic thermal conduction losses from heater to cooler

The heat losses related the parasitic thermal conduction from heater to cooler ($\dot{Q}_{loss,cnd}$) are evaluated as a simple conduction phenomenon because the temperature of the two parts is constant during the engine operation:

$$\dot{Q}_{loss,cnd} = \frac{S \cdot (T_h - T_k) \cdot K_{cd}}{L}$$

where S stands for average the cross section of the walls (about 7 cm^2 in the studied engine), K_{cd} for conduction coefficient (25 W/m K) and L for the axial length of the regenerator walls (2 cm).

References

[1]

N.C.J. Chen and F.P. Griffin, A review of stirling engine mathematical models, 1983, Oak Ridge National Laboratory.

[2]

C.H. Cheng and Y.J. Yu, Numerical model for predicting thermodynamic cycle and thermal efficiency of a beta-type Stirling engine with rhombic-drive mechanism, *Renewable Energy* **35**, 2010, 2590–2601.

[3]

I. Urieli and D.M. Berchowitz, Stirling cycle engine analysis, 1984, Adam Hilger Ltd; Bristol.

[4]

T. Finkelstein and A.J. Organ, The air engines, 2001, The American Society of Mechanical Engineers; New York.

[5]

S. Schulz and F. Schwendig, A general simulation model for Stirling cycles, *Gas Turbines Power* **118**, 1996, 1–7.

[6]

B. Kongtragool and S. Wongwises, A review of solar-powered Stirling engines and low temperature differential Stirling engines, *Renew Sustain Rev* **7**, 2003, 131–154.

[7]

H. Karabulut, Dynamic analysis of a free piston Stirling engine working with closed and open thermodynamic cycles, *Renewable Energy* **36**, 2011, 1704–1709.

[8]

N. Parlak, A. Wagner, M. Elsner and H.S. Sohyan, Thermodynamic analysis of a gamma type Stirling engine in non-ideal adiabatic conditions, *Renewable Energy* **34**, 2009, 266–273.

[9]

S.K. Andersen, H. Carlsen and P.G. Thomsen, Control volume based modelling in one space dimension of oscillating, compressible flow in reciprocating machines, *Simul Model Pract Theory* **14**, 2006, 1073–1086.

[10]

A.J. Organ, The regenerator and the Stirling engine, 1997, Mechanical Engineering Publications Limited; London.

[11]

K. Mahkamov, Design improvements to a biomass Stirling engine using mathematical analysis and 3D CFD modeling, *J Energy Res Technol* 2006, 128–203.

[12]

Y. Timoumi, I. Tlili and S.B. Nasrallah, Design and performance optimization of GPU-3 Stirlingengines, *Energy* **33**, 2008, 1100–1114.

[13]

G. Walker, Stirling engines, 1980, Clarendon Press; Oxford.

[14]

Wilson SD, Dyson RW, Tew RC, Ibrahim MB. Multi-D CFD modeling of a free-piston stirling convertor at NASA Glenn, NASA/TM-2004-213351 AIAA-2004-5673.

[15]

M. Costea, S. Petrescu and C. Harman, The effect of irreversibilities on solar Stirling cycle performance, *Energy Convers Manage* **40**, 1990, 1723–1731.

[16]

Gedeon D, Wood JG. Oscillating-Flow Regenerator Test Rig: Hardware and Theory With Derived Correlations for Screens and Felts, NASA Contractor Report 198442; 1996.

[17]

S.C. Costa, H. Barrutia, J.A. Esnaola and M. Tutar, Numerical study of the pressure drop phenomena in wound woven wire matrix of a Stirling regenerator, *Energy Convers Manage* **67**, 2013, 57–65.

[18]

C.H. Cheng and H.S. Yang, Optimization of geometrical parameters for Stirling engines based on theoretical analysis, *Appl Energy* **92**, 2012, 395–405.

[19]

A. Aliabadi, M.J. Thomson, J.S. Wallace, T. Tzanetakis, W. Lamont and J. Di Carlo, Efficiency and emissions measurement of a stirling-engine-based residential microcogeneration system run on diesel and biodiesel, *Energy Fuels* **23**, 2009, 1032–1039, http://dx.doi.org/10.1021/ef800778g.

[20]

D. García, M.A. González, J.I. Prieto, S. Herrero, S. López, I. Mesonero, et al., Characterization of the power and efficiency of Stirling engine subsystems, *Appl Energy* **121**, 2014, 51–63.

[21]

G. Valenti, P. Silva, N. Fergnani, G. Di Marcoberardino, S. Campanari and E. Macchi, Experimental and numerical study of a micro-cogeneration Stirling engine for residential applications, *Energy Procedia* **45**, 2014, 1235–1244, http://dx.doi.org/10.1016/j.egypro.2014.01.129.

[22]

S. Campanari, G. Valenti, E. Macchi, G. Lozza, N. Ravidà and N. Lazzari, Development of a microcogeneration laboratory and testing of a natural gas CHP unit based on PEM fuel cells, *Appl Therm Eng* **71**, 2014, 714–720, http://dx.doi.org/10.1016/j.applthermaleng.2013.10.067.

[23]

International Organization for Standardization, ISO/IEC GUIDE 98–3:2008(E) Uncertainty of measurement Part 3: Guide to the expression of uncertainty in measurement (GUM:1995).

[24]

B. Thomas, Benchmark testing of Micro-CHP units, *Appl Therm Eng* **28**, 2008, 2049–2054, http://dx.doi.org/10.1016/j.applthermaleng.2008.03.010.

Footnotes

[1]In this work, the term "Stirling engine" refers strictly to the engine itself, while "Stirling unit" to the combination of the engine and the ancillaries used in a cogeneration installation, as for instance burner, fan, cogeneration heat exchanger, air preheating, etc.

Highlights

- A Stirling rated at 1 kWe and 8 kWth is analyzed experimentally and numerically.

- The developed model is an extension of the work by Urieli and Berchowitz.

- The initial pressure of the working fluid (nitrogen) is varied from 9 to 24 bar_g.

- The initial pressure influences strongly the fuel input and the electrical power.

- Major losses: wall heat conduction and non-unitary regenerator effectiveness.

Queries and Answers

Query: Your article is registered as belonging to the Special Issue/Collection entitled "ICAE2014". If this is NOT correct and your article is a regular item or belongs to a different Special Issue please contact h.moorthy@elsevier.com immediately prior to returning your corrections.
Answer: The information is correct, the paper belongs to "ICAE2014"

Query: Please confirm that given name(s) and surname(s) have been identified correctly.
Answer: Confirm all names

elsevier_APEN_6627

Query: The decimal commas have been changed to a decimal points in Table [1]. Please check, and correct if necessary.

Answer: Thanks for the correction. I confirm it is fine now.